Acta metall. mater. Vol. 41, No. 2, pp. 345–360, 1993
Printed in Great Britain.

0956-7151/93 $6.00 + 0.00

PROBABILISTIC MODELLING OF MICROSTRUCTURE FORMATION IN SOLIDIFICATION PROCESSES

M. RAPPAZ and Ch.-A. GANDIN

Laboratoire de Métallurgie Physique, Ecole Polytechnique Fédérale de Lausanne, MX-G, CH-1015 Lausanne, Switzerland

(Received 25 March 1992; in revised form 1 July 1992)

Abstract—A new approach to the modelling of grain structure formation in solidfication processes is proposed. Based upon a two-dimensional cellular automata technique, the model includes the mechanisms of heterogeneous nucleation and of grain growth. Nucleation occurring at the mould wall as well as in the liquid metal are treated by using two distributions of nucleation sites. The location and the crystallographic orientation of the grains are chosen randomly among a large number of cells and a certain number of orientation classes, respectively. The growth kinetics of the dendrite tip and the preferential ⟨100⟩ growth directions of cubic metals are taken into account. The model is then applied to small specimens of uniform temperature. The columnar-to-equiaxed transition, the selection and extension of columnar grains which occur in the columnar zone and the impingement of equiaxed grains are clearly shown by this technique. The calculated effect of the alloy concentration and cooling rate upon the resultant microstructure agree with experimental observations.

Résumé—Une nouvelle approche est proposée pour modéliser la formation de microstructures de solidification. Se basant sur une technique d'automate cellulaire bi-dimensionnel, le modèle tient compte des mécanismes de germination hétérogène et de croissance de grains. La germination est décrite par deux distributions de sites appliquées sur les parois du moule et dans le métal liquide. La localisation et l'orientation cristallographique des grains sont choisies aléatoirement parmi un grand nombre de cellules et de classes d'orientation, respectivement. La cinétique de croissance de la pointe de la dendrite et les directions de croissance ⟨100⟩ préférentielles des métaux cubiques sont reproduites. Le modèle est appliqué à de petits échantillons de température uniforme. La transition colonnaire-équiaxe, la sélection et la propagation des grains colonnaires ainsi que la rencontre des grains équiaxes sont clairement reproduits par cette technique. Les effets de la concentration de l'alliage et de la vitesse de refroidissement sur la microstructure simulée s'accordent avec les observations expérimentales.

Zusammenfassung—Ein neues Verfahren zur Modellisierung der Kornstruktur bei Erstarrungsprozessen wird vorgeschlagen. Basierend auf einer zweidimensionalen Zellularautomatentechnik berücksichtigt das Modell die Mechanismen der heterogenen Keimbildung und des Kornwachstums. Keimbildung an der Wand sowie im flüssigen Metall werden mit jeweils verschiedenen Verteilungsfunktionen der Keimdichte behandelt. Die Orte für die Kornentstehung werden statistisch aus einer grossen Zahl von Zellen bestimmt. Ebenso wird die kristallographische Orientierung der Körner statistisch aus einer bestimmten Zahl von Orientierungsklassen ausgewählt. Die Wachstumskinetik der Dendritenspitzen sowie das bevorzugte Wachstum kubischer Metalle in ⟨100⟩ Richtung werden berücksichtigt. Das Modell wird auf kleine Proben mit gleichförmiger Temperaturverteilung angewandt. Der Übergang von säulenförmigem zu globularem Wachstum, die Kornauswahl und das Wachstum säulenförmiger Kristalle sowie das Aufeinanderstossen globularer Körner werden von dieser Technik klar simuliert. Die Berechnungen des Einflusses von Legierungskonzentration und Abkühlgeschwindigkeit auf das resultierende Gefüge stimmen gut mit den experimentellen Beobachtungen überein.

1. INTRODUCTION

Software tools for the simulation of solidification processes have become increasingly sophisticated [1]. At the macroscopic scale, the use of finite difference (FDM) or finite element (FEM) methods allows one to calculate heat and mass transfer in complex two- or three-dimensional geometries, for transient or stationary situations. However, when using most of these approaches, the mushy region within which alloy solidification occurs is over-simplified. In macroscopic methods based upon average continuity equations [2–5], it is usually assumed that solidification starts at the liquidus and finishes at the solidus or eutectic temperatures, the details of microstructure formation being obscured. This is because the scale of the microstructure is much smaller than that of the overall process, since it is dictated primarily by solute diffusion and capillarity effects.

On the other hand, microscopic models of solidification have been developed which take account of the mechanisms of grain nucleation and grain growth in alloys which are solidifying with equiaxed dendritic or eutectic microstructures [6]. Most of these models are based upon a deterministic approach which can be summarised as follows: the density of grains which

have nucleated in the bulk liquid at a given moment during solidification is a function of the undercooling. This function, which cannot be found from theoretical considerations alone, is deduced from a set of experiments (e.g. measurement of the cooling curve and of the grain density, as seen in micrographic cross-sections, for specimens solidified at various cooling rates). As soon as a grain has nucleated, it grows with an interface velocity which is also a function of the undercooling. In this case, the solidification kinetics of the dendrite tips or of the eutectic interface can be deduced from theoretical models [7, 8]. The impingement of the grains, which is very important for eutectic microstructures, has typically been treated by using the standard Avrami–Johnson–Mehl correction [9, 10] or by using geometrical [11, 12] or random [13] grain arrangement models. These microscopic models of solidification have been coupled with macroscopic heat flow calculations in order to predict successfully the microstructural features, in particular the grain size, at the scale of the whole process [14–16]. The growth of columnar microstructures, which is initiated by nuclei that form at the mould surface, is usually simulated in a much simpler way. By using the same models for the growth kinetics [7, 8], the undercooling of the eutectic front or that of the dendrite tips, as well as the lamellae or dendrite trunk spacings, are directly deduced from the thermal gradient and the speed of the corresponding isotherm (eutectic or liquidus, respectively). The latter values are obtained from a macroscopic heat flow calculation [6]. The secondary arm spacings of both equiaxed and columnar dendritic microstructures are deduced from the local solidification time [17].

However, the value of these "deterministic" solidification models is limited. Since they neglect any aspect which is related to crystallographic effects, they cannot account for the grain selection which occurs close to the mould surface and which gives rise to the columnar region. It is well known that, for cubic metals, this selection is based upon a criterion of "best alignment" of the $\langle 100 \rangle$ crystallographic axes of the grain with the heat flow direction [18–20]. Therefore, these models are unable to predict the so-called "equiaxed-columnar" transition, which occurs near to the mould wall [18], or the variation of the transverse size of columnar grains [19]. These aspects are particularly important in the directional solidification (DS) or the production of single crystal dendritic alloys for aerospace applications. The extension of a grain into an open region of liquid is another important phenomenon which can hardly be accounted for by using these methods. Finally, the transition from a columnar to an equiaxed (CET) microstructure, which occurs in the bulk liquid when the thermal gradient is small, is also difficult to model with the aid of these deterministic approaches [21].

Realizing the limitations of deterministic models for solidification, Brown and Spittle have developed a totally different approach which is based upon a "probabilistic" concept [22–24]. These authors have adapted, to the case of solidification, the Monte Carlo procedure which had been developed by Srolovitz *et al.* [25] for treating grain growth. This type of method is based upon minimisation of the interfacial energy, as achieved by considering the energy of unlike sites (e.g. liquid/solid sites or sites belonging to different grains) and by allowing transitions between these states to occur according to randomly generated numbers. By using this method, Brown and Spittle were able to produce computed two-dimensional microstructures which resembled very closely those observed in real micrographic cross-sections. In particular, the selection of grains in the columnar zone, and the CET transition, were reproduced nicely by using this technique. These authors could also qualitatively demonstrate the effect of solute concentration or melt superheat upon the resultant microstructure. However, as noted by these authors, these methods suffer considerably from the lack of a physical basis and thus cannot be used to analyze quantitatively the effects of the various physical phenomena. For example, during one Monte Carlo time step, the N sites whose evolution is calculated are chosen randomly among the N Monte Carlo sites and therefore not all the sites of interest (i.e. those located near to the solid–liquid interface) are investigated. The grain competition in the columnar region, as predicted by their algorithm, does not at all reflect the physical mechanisms which are observed in organic alloys [26]. Furthermore, the results are sensitive to the type of Monte Carlo network which is used for the computations.

The purpose of the present contribution is to combine, in a single model, the advantages of probabilistic methods with those of deterministic approaches so as to predict more accurately the grain structure in castings. For that purpose, a two-dimensional cellular-automata-type simulation, which is based upon the physical mechanisms of nucleation and growth of dendritic grains, has been developed. Heterogeneous nucleation, which was modelled by means of a nucleation site distribution in deterministic solidification models, is treated in a similar way in the present probabilistic approach. If the total density of grains which nucleate at a given undercooling is obtained from an average distribution, the location of these sites is chosen randomly. The random crystallographic orientation of a newly nucleated grain is also taken into account. As will be shown, the growth kinetics of the dendritic tips and of the side branches are incorporated into the model in such a way that the final simulated microstructure is independent of the cellular automaton network which is used for the computations. Although it produces micrographic cross-sections which are similar to those already obtained by Brown and Spittle, the present model has a sound physical basis and can thus reflect quantitat-

ively the effects of cooling rate or solute concentration.

2. PHYSICAL BACKGROUND

Figure 1 shows an experimental micrographic cross-section for an aluminium–7% silicon ingot, cast in a ceramic mould over a copper chill-plate [6]. The dendritic grains, which have various crystallographic orientations, appear as zones of differing greyness. As can be seen, the three typical regions which are encountered in most solidification processes [18, 19] are present in this micrograph. At the bottom of the ingot, very small grains are nucleated at the surface of the copper chill (outer equiaxed region). After these grains have nucleated, they grow towards the top of the casting and this results in the so-called columnar region (lower half of the casting shown in Fig. 1). These columnar grains would extend up to the top of the casting if they were not stopped by equiaxed grains which nucleate in the bulk of the liquid (upper half of the casting shown in Fig. 1).

The transition from a columnar to an equiaxed microstructure (CET) has been analyzed by Flood and Hunt [21] with the aid of a deterministic solidification model that included the effect of convection. The transition from the outer equiaxed region to the columnar zone, as well as the grain selection which occurs in the lower half of the casting shown in Fig. 1, can be understood in terms of anisotropic growth effects [18, 19]: that is, those grains which have one of their $\langle 100 \rangle$ crystallographic orientations most closely aligned with the heat flow direction out-grow those which have a less favourable orientation. This selection mechanism has been observed *in situ* for organic alloys by Esaka *et al.* [26], but further evidence is provided by metallic alloys [19, 20]. In fact, this selection process is routinely used

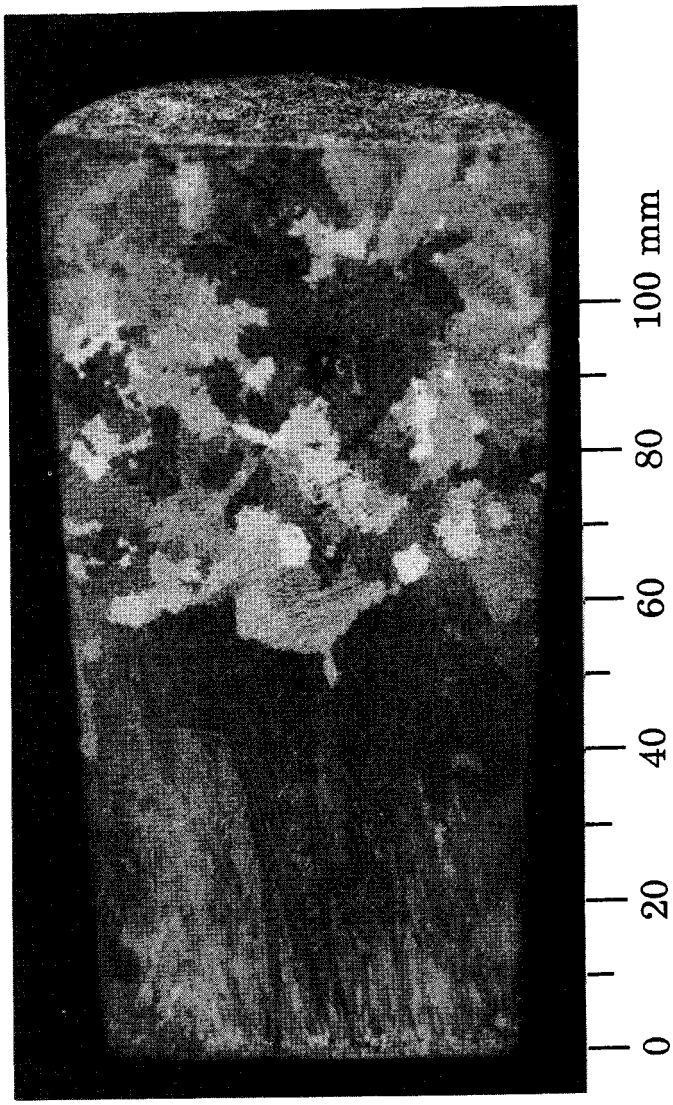

Fig. 1. Experimental micrographic cross-section of an aluminium–7% silicon alloy which was cast over a copper chill-plate under unidirectional heat flow conditions (after Ref. [6]).

for the production of single-crystal turbine blades [27]. As schematically shown in Fig. 2, the "best alignment" selection criterion for dendritic grains corresponds to a minimum undercooling criterion. In this figure, the two grains on the left and on the right contain dendrites whose ⟨100⟩ trunk orientation is nearly perpendicular to the liquidus isotherm. Therefore, in a quasi-stationary situation, these dendrites grow with the same velocity, v_L, as that of liquidus isotherm. For the grain in the middle of the figure, the ⟨100⟩ crystallographic direction has a misorientation, θ, with respect to the heat flow direction. The corresponding dendrite trunks that grow with this orientation must therefore have a velocity, $v_\theta = v_L/\cos(\theta)$, which is larger than v_L in order to keep up with the liquidus isotherm. According to the growth kinetics model for the dendrite tip [7], they are therefore characterized by a slightly larger undercooling and lie behind the better oriented dendrites (i.e. $\Delta z_\theta > \Delta z_0$ in Fig. 2). This small lag will cause the dendrites to be out-grown by those having a better orientation. This might occur in two different ways. If the ⟨100⟩ orientations of the two neighbouring grains are converging (the situation for the two grains shown on the left of Fig. 2), the dendrite tips of the less-favourably oriented grain hit the side of the best-aligned grain and are stopped. When the ⟨100⟩ growth orientations are diverging (the situation for the two grains shown on the right of Fig. 2), an open region of liquid is always available at the grain boundary. The extension of secondary dendrite arms into this region, which is similar to that which occurs near to a mould wall, is discussed below.

The extension of one grain into an open region of liquid might occur near to the mould wall when the dendrite trunk orientation diverges from the mould surface or when the cross-section of the mould varies (see left of Fig. 2). The same mechanism operates in the liquid region which is located between two grains having divergent ⟨100⟩ orientations (the two grains on the right of Fig. 2). In both cases, the branches of the dendrite near to the mould wall, or near to the grain boundary, no longer meet any obstacle to the rejection of solute into the melt and can thus extend further into the liquid. The extension of these secondary arms into these open regions of liquid is complex because, as shown by Esaka *et al.* [26], their growth kinetics is neither that of a parabolic tip nor that of a parabolic cylinder. For a certain distance, or "incubation time", behind the tip all of the secondary arms grow side-by-side with almost the same velocity and thus the solute fields which are associated with rejection at the branch tips overlap. After this incubation period, one of these dendrite arms can "escape" from its neighbours due to some random fluctuation (thermal, solutal, morphological), i.e. the solute which is rejected by the tip of this dendrite arm will no longer interfere with that of its neighbours. From that point on, its growth kinetics will be close to that of an isolated tip. In a positive temperature gradient, the undercooling at which this branch grows, and thus its growth rate, is larger than that of the primary dendrite tip itself. The extension of this secondary dendrite arm is accompanied by the development of tertiary branches which, after some selection mechanism has operated, can become new

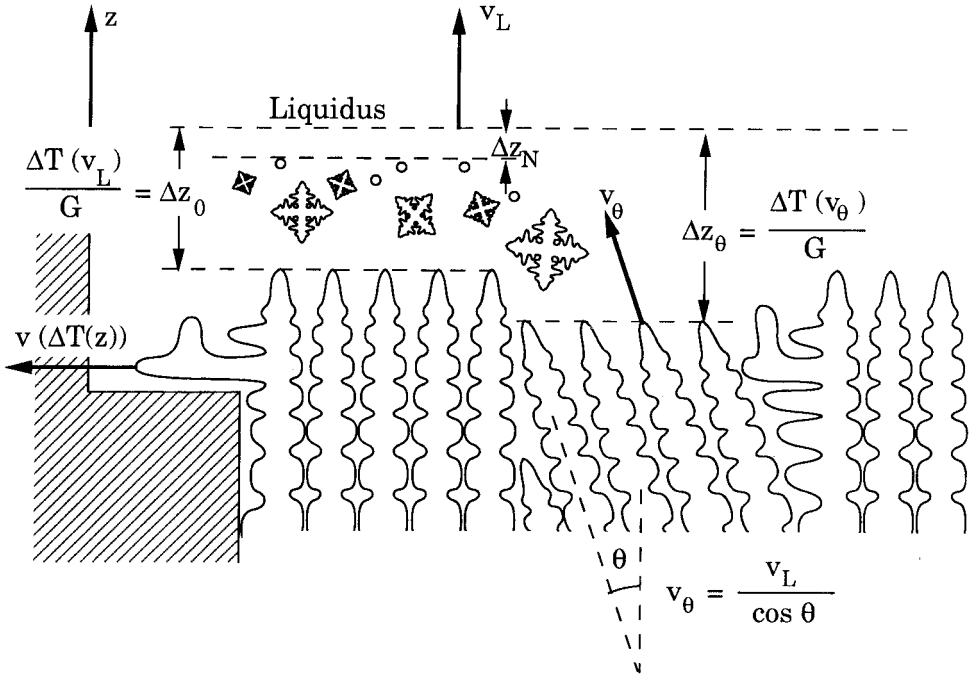

Fig. 2. Schematics for the various growth mechanisms occurring in a dendritic alloy with a non-uniform temperature.

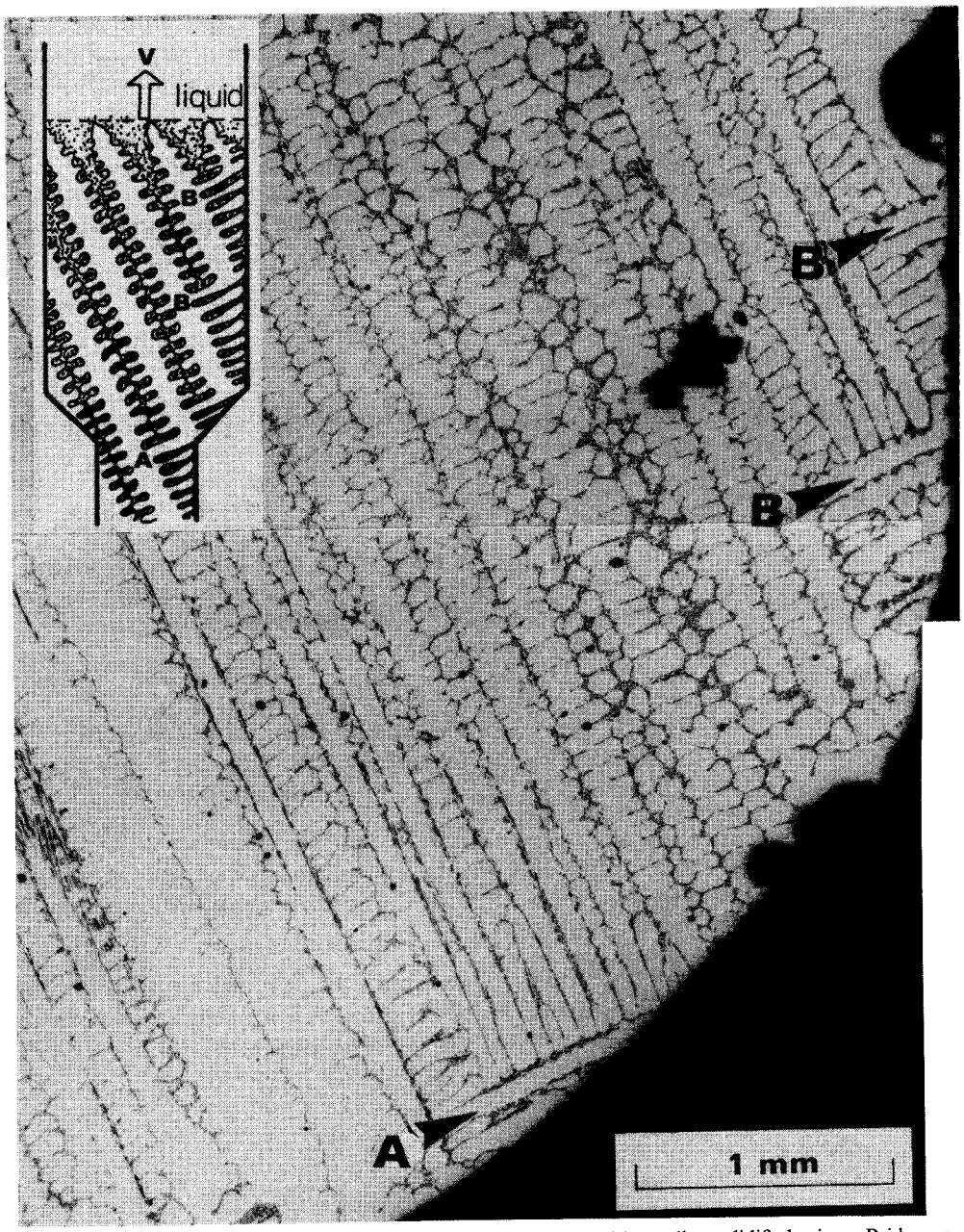

Fig. 3. Longitudinal micrograph of a dendritic single crystal nickel-base alloy solidified using a Bridgman technique and showing, at locations labeled A and B, the extension of secondary arms into open liquid (after Ref. [20]).

primary dendrite trunks, as shown schematically in Fig. 2. The result of this branching mechanism is illustrated in Fig. 3 for a directionally solidified Ni–Cr–C ingot [20] (see regions labeled "A" and "B").

The final mechanism involved in dendritic grain formation is that shown in Fig. 2: the heterogeneous nucleation of new grains in the supercooled liquid region ahead of the columnar dendrites. Such nucleation can be enhanced by the intentional addition of particles of inoculant to the melt (e.g titanium-boride for aluminium alloys) [28] or by the detachment of existing dendrite arms due to convection or to thermal fluctuations [29]. In both cases, these newly nucleated grains can stop the growth of columnar dendrites; thus resulting in a CET transition, as analyzed by Flood and Hunt [21]. After a certain period of growth during which a newly nucleated grain grows with an almost spherical shape [30], an instability usually develops and the equiaxed grain becomes dendritic†. Provided that the thermal

†When the grain density is large, the solute layer of one grain might overlap that of its neighbours before the grains become dendritic. This so-called "globulitic" morphology will be ignored here.

undercooling is small, which is a good approximation for most metallic alloys when solidified under normal solidification conditions, the growth kinetics of the equiaxed dendritic tip is close to that of the columnar dendrite [7]. Thus, the radius of an equiaxed grain at a given time is given by the integral, of the velocity of its dendrite tips, from the time of nucleation to that of observation (see Fig. 2).

To sum up, if the incubation times required for a spherical grain to become dendritic, or for a dendrite arm to detach from its neighbours, are neglected the final grain structure that is observed in a casting is determined by three main phenomena: the heterogeneous nucleation of grains at the mould wall and in the bulk of the melt; the preferential growth orientations which, for cubic metals, correspond to $\langle 100 \rangle$ crystallographic directions and finally the growth kinetics of a dendrite tip, which can be calculated from the KGT model. These three aspects are described in detail below.

Heterogeneous nucleation

Deterministic models of solidification have shown that, at the small undercoolings encountered in conventional solidification processes, the theory of heterogeneous nucleation with a single type of nucleation site [31] has difficulty in accounting for the grain-size dependence which is seen in metallographic cross-sections [6]. This is due to the fact that nucleation occurs almost instantaneously, and quickly saturates all of the sites, at a critical undercooling. Thus, more than one type of nucleation site was assumed to exist in most microscopic models of solidification; each of these site families becoming active at a critical undercooling [6, 32, 33]. Following the pragmatic approach of Oldfield [32], a continuous nucleation distribution, $dn/d(\Delta T)$, can be used to describe the grain density increase, dn, which is induced by an increase in the undercooling, $d(\Delta T)$. Therefore, the total density of grains, $n(\Delta T)$, which have been nucleated at a given undercooling, ΔT, is given by the integral of this distribution

$$n(\Delta T) = \int_0^{\Delta T} \frac{dn}{d(\Delta T')} d(\Delta T'). \quad (1)$$

If the extinction of nucleation sites by the growing grains is taken into account [33], then equation (1) transforms to

$$n(\Delta T) = \int_0^{\Delta T} \frac{dn}{d(\Delta T')} [1 - f_s(T')] d(\Delta T') \quad (2)$$

where f_s is the volume fraction of solid already formed.

Oldfield has used a simple polynomial law with two parameters in order to describe the nucleation of cast iron. Some authors have used the same approach [14, 15, 32, 33] while others have used a Gaussian function with three parameters [12, 16]. In the present work, Gaussian distributions will be used to describe heterogeneous nucleation both at the mould surface and in the bulk of the melt. Two such functions are shown in Fig. 4. The density of sites at the mould wall has the units of m^{-2} whereas that in the volume of the melt has the units of m^{-3}. The characteristics of these two distributions (mean undercooling, ΔT_{max}, standard deviation, ΔT_σ, and total density of grains, n) can only be determined via exponential observations, as already shown in deterministic approaches of solidification [6].

Dendrite growth orientation

The preferred dendrite growth directions of cubic metals are along the $\langle 100 \rangle$ crystallographic orientations [18, 19]. As the cellular automaton presented here is two-dimensional, only four such orientations with just two Miller indices, $\langle 10 \rangle$, will be considered here. Grains which are nucleated either at the mould surface or in the volume of the melt are assumed to have a random crystallographic orientation. Thus, the probability, $dp(\theta)$, that a newly nucleated grain has a principal growth direction in the range $[\theta, \theta + d\theta]$ is simply given by

$$dp(\theta) = \frac{2}{\pi} d\theta. \quad (3)$$

The constant takes into account the four-fold symmetry of the dendrite (i.e. the integral of $dp(\theta)$ from $-\pi/4$ to $+\pi/4$ is equal to unity).

Dendrite tip growth kinetics

In castings, the total undercooling of the dendrite tip, ΔT, is generally the sum of four contributions [34]

$$\Delta T = \Delta T_c + \Delta T_t + \Delta T_k + \Delta T_r \quad (4)$$

where ΔT_c, ΔT_t, ΔT_k and ΔT_r are the undercooling contributions associated with solute diffusion, thermal diffusion, attachment kinetics and solid–liquid

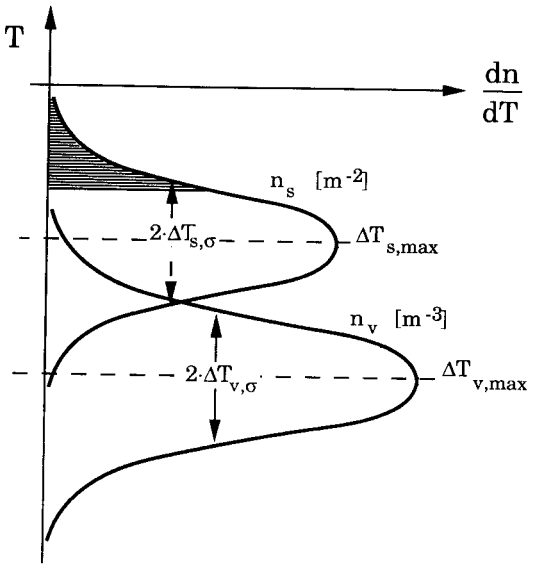

Fig. 4. Nucleation site distributions for nuclei formed at the mould wall and in the bulk of the liquid.

interface curvature, respectively. For most metallic alloys, when solidified under normal solidification conditions, the last three contributions that appear on the RHS of equation (4) are small, and solute undercooling predominates. Thus, the growth kinetics of both columnar and equiaxed morphologies can be calculated with the aid of the KGT model [7]. The result of using this model is shown in Fig. 5 for two aluminium–silicon alloys of different concentrations (5 and 7%). Without giving all of the details of the KGT model (which can be found in Ref. [7]), it is recalled that the dendrite tip radius, R, and velocity, v, are determined by the two relationships

$$\Omega = \frac{c^* - c_0}{c^*(1-k)} = \mathrm{Iv(Pe)} \tag{5}$$

and

$$R = 2\pi\sqrt{\left(\frac{\Gamma}{mG_c\xi_c - G}\right)} \tag{6}$$

where the solutal Péclet number, Pe, is given by

$$\mathrm{Pe} = \frac{Rv}{2D} \tag{7}$$

Ω is the supersaturation, c_0 is the initial concentration of the alloy, c^* is the concentration in the liquid at the tip, k is the partition coefficient, m is the slope of the liquidus, D is the diffusion coefficient in the liquid, Γ is the Gibbs–Thomson coefficient, and G_c is the solute gradient in the liquid at the tip. In the dendritic regime, the thermal gradient, G, can be neglected [7]. Iv(Pe) is the Ivantsov function of the Péclet number and ξ_c is also a function of the Péclet number which, at low growth rates, is close to unity.

The undercooling, ΔT, is related to the supersaturation, Ω, by the relationship

$$\Delta T = mc_0\left[1 - \frac{1}{1-\Omega(1-k)}\right]. \tag{8}$$

Therefore, the relationship between the growth rate of the dendrite tip, v, and its undercooling, ΔT, is given by the solution of equations (5)–(8) [7]. As can be seen in Fig. 5, the growth rate of the dendrite tip at a given undercooling decreases with increasing alloy concentration.

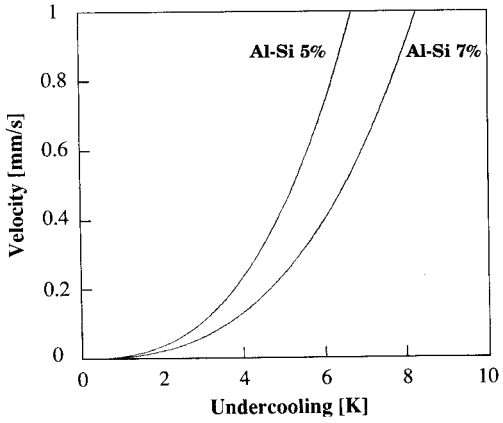

Fig. 5. Growth kinetics of a dendrite tip, as calculated using the KGT model, for two aluminium–silicon alloys of differing composition.

The probabilistic modelling of grain formation in castings is first developed for thin plates or small square slabs under the assumption of a uniform temperature field. This occurs when the Biot number, Bi, of the specimen is small, i.e. when $\mathrm{Bi} = hL/\kappa \ll 1$. Here, h is the heat transfer coefficient, L is a characteristic dimension of the specimen and κ is the thermal conductivity of the alloy. Under this assumption, and provided that the thermal undercooling, ΔT_t, can be neglected [see equation (4)], the undercooling of the dendrite tips and arms is the same everywhere. As the curvature and kinetic undercoolings are rather small under normal solidification conditions, this means that the entire dendritic pattern is close to an isoconcentrational surface (ΔT_c constant). This situation is shown schematically in Fig. 6(a) for a thin plate. The axis of symmetry of the plate is near to the top of the figure, and the mould wall is at the bottom. Under the assumption of a uniform temperature, there is no clear distinction between the grains which are nucleated at the mould wall and those which are formed in the bulk of the melt; except that the first ones can only extend into the upper half-space above the mould surface. For the sake of simplicity, the grains which are nucleated at the mould surface will be called "columnar", because they may eventually be elongated grains when solidification is complete, whereas "equiaxed" grains are nucleated in the volume of the melt (see Fig. 1). If the incubation time which is necessary for a dendrite arm to take over its neighbours is neglected, then the overall shape of an equiaxed grain can be approximated by a square in two dimensions, whose main diagonals correspond to the ⟨10⟩ crystallographic directions. *In situ* observations of organic alloys [35] have shown that the overall shape of an equiaxed grain is, in fact, slightly concave and that the concavity increases with increasing solute concentration. This will be neglected in the case of the cellular automaton which is presented here.

3. A PHYSICALLY-BASED CELLULAR AUTOMATON

According to Hesselbarth and Göbel, who modelled recrystallization [36], a cellular automaton obeys the following rules: (i) the space is divided into cells of equal size, usually squares or hexagons in two dimensions, arranged in a regular lattice; (ii) the neighbourhood of each cell is defined (e.g. first-, or first- and second-nearest neighbours); (iii) each cell is characterized by different variables (e.g. temperature, crystallographic orientation) and states (e.g. liquid, solid); (iv) the rules of transition (e.g. liquid to solid) which determine the evolution of a given cell during one time step are defined according to the variables

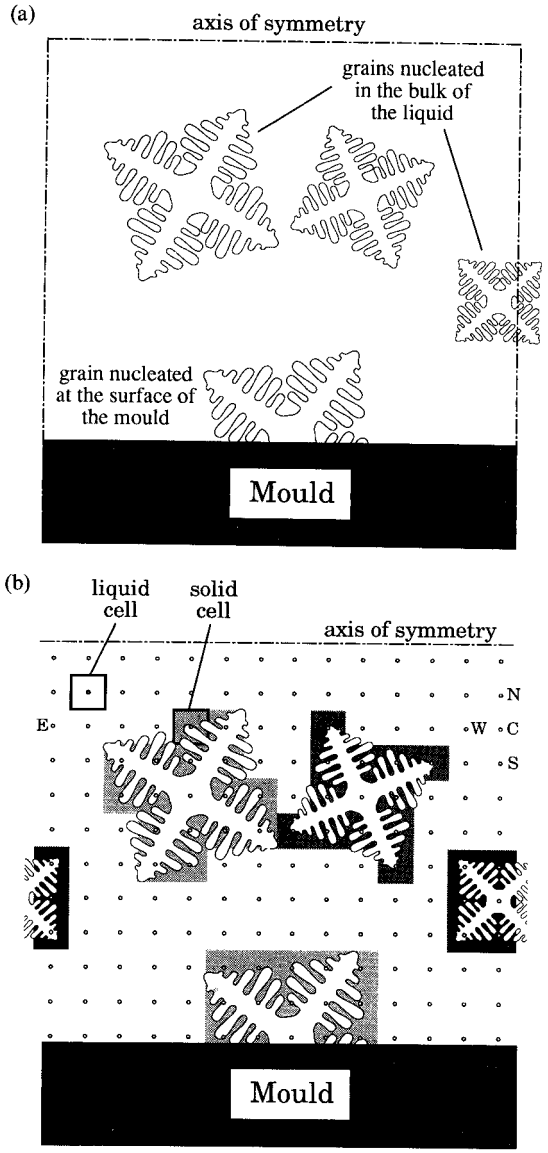

Fig. 6. (a) Schematics for a small solidifying volume element of uniform temperature within which nucleation and growth can occur from the mould wall and in the bulk. (b) Schematics for the cellular automaton used to predict microstructure formation in the small solidifying specimen shown in (a).

and/or states of the neighbouring cells. In order to simulate grain formation for the situation which is shown schematically in Fig. 6(a), time-stepping cellular automaton (CA) was developed as described below.

Firstly, a network of cells is laid out according to a regular lattice arrangement [see Fig. 6(b)]. In two dimensions, two types of lattices were tried: cubic and hexagonal. Only the cubic lattice is shown in Fig. 6(b). In the simplest CA configuration, only the nearest-neighbour cells of a site location are considered: for the cubic lattice, this corresponds to the cells at the North, South, West and East of the site C in Fig. 6(b) (indices N, S, W, E). Since the plate is cut arbitrarily by two planes perpendicular to the mould surface [see Fig. 6(a)], periodic conditions are set on these boundaries. Therefore, the cells on the right boundary have their east neighbour located on the left boundary and vice versa [see Fig. 6(b)]. At the beginning of the simulation, each cell is given the same initial temperature above the liquidus of the alloy and a state index equal to zero; meaning that it is liquid. The sites which are located immediately next to the mould wall have a reference number which indicates that they belong to this boundary. The time-stepping calculation is then started. The temperature at each time-step is given by the cooling curve of the specimen, which is obtained either from a heat-flow computation or from a temperature measurement. When the temperature becomes lower than the liquidus point, the cells can become solid, as governed by the two mechanisms, of heterogeneous nucleation and growth, as described above. The locations of new nuclei are chosen at random among all of the remaining liquid cells. In a similar way, the crystallographic orientation of a new nucleus is chosen randomly among equi-probabilistic orientation classes. The entrapment of a liquid cell by the growth of an existing solid neighbour is also treated by using a Monte Carlo procedure. These aspects are detailed below.

Nucleation

During one time-step, δt, the temperature of the specimen decreases by an amount, δT, and thus the undercooling increases by an amount $\delta(\Delta T)$ [$\delta(\Delta T) > 0$]. Accordingly, the density of new grains which are nucleated within the volume of the melt is given by [see equation (1)]

$$\delta n_v = n_v[\Delta T + \delta(\Delta T)] - n_v(\Delta T) = \int_{\Delta T}^{\Delta T + \delta(\Delta T)} \frac{\mathrm{d}n_v}{\mathrm{d}(\Delta T')}\,\mathrm{d}(\Delta T') \qquad (9)$$

where the index "v" refers to the nucleation site distribution for the volume of the melt (see Fig. 4). This grain density increase, δn_v, multiplied by the total volume of the specimen, V, gives the number of grains, δN_v, which are nucleated during the time step, δt. The location of these new grains is randomly chosen among all the CA sites by defining the corresponding probability, p_v, that a cell nucleates during the time step δt, i.e.

$$p_v = \frac{\delta N_v}{N_{CA}} = \delta n_v V_{CA} \qquad (10)$$

N_{CA} is the total number of cells used to represent the volume V and V_{CA} is the volume associated with one CA cell. During the time step, δt, all of the cells defining the volume of the specimen are scanned and a random number, r, is generated for each of them ($0 \leqslant r \leqslant 1$). The nucleation of a cell which is still liquid, i.e. whose index is still equal to zero will occur only if

$$r \leqslant p_v. \qquad (11)$$

If the cell effectively transforms from liquid to solid by nucleation, its corresponding index is defined to be a positive integer. This value, which represents its crystallographic orientation, is again chosen randomly among a certain number of classes of possible orientations. In two dimensions, it was found that 48 classes were enough to produce a grain structure which was sufficiently close to the real microstructures observed in micrographic cross-sections. Indeed, for the four-fold symmetry of the dendritic grain, 48 classes of orientation correspond to a class width of less than 2°.

A few comments can be made at this stage. The probability, p_v, should not be too large and in any case should never exceed unity. If this was the case, it would mean that the density of CA points was not large enough to represent the very fine grain size of the structure. It should also be noted that the method described above for the handling of heterogeneous nucleation already takes account of the extinction of nucleation sites due to the formation of solid [see equation (2)]. Indeed, equation (10) contains the total number of CA sites and not the number of cells which remain liquid at this time. Finally, a similar procedure is applied to the heterogeneous nucleation of grains at the surface of the mould. In this case, the grain density increase, δn_s, which occurs during the time step, δt, is calculated by using a relationship similar to equation (9) together with the surface nucleation site distribution (see Fig. 4). The total number of grains nucleated at the surface of the mould, δN_s, is then obtained by multiplying δn_s by the active surface area of the mould, S, and the corresponding probability, p_s, is then given by the ratio of δN_s over the total number of CA cells which are located near to the mould wall.

Growth

Although the generation of the random nucleation site locations is quite easy, the treatment of the growth stage by means of cellular automata is more difficult. In particular, it is well known that the configuration of the CA network has a direct influence upon the simulated microstructure. Srolovitz *et al.* [25] and later Brown and Spittle [22–24] used a hexagonal, rather than a square, two-dimensional lattice in order to better leverage the anisotropy induced by the directions of the nearest-neighbours.

In the present work, it was desired to design a probabilistic model which would fulfil three requirements: firstly, the outcome of the model had to be independent of the CA network used; secondly, the model had to reflect the preferential ⟨100⟩ growth directions, which have a random orientation with respect to the orientation of the nearest neighbour cells; and thirdly, the growth kinetics of the dendrite tips had to be taken into account properly. This was achieved as follows.

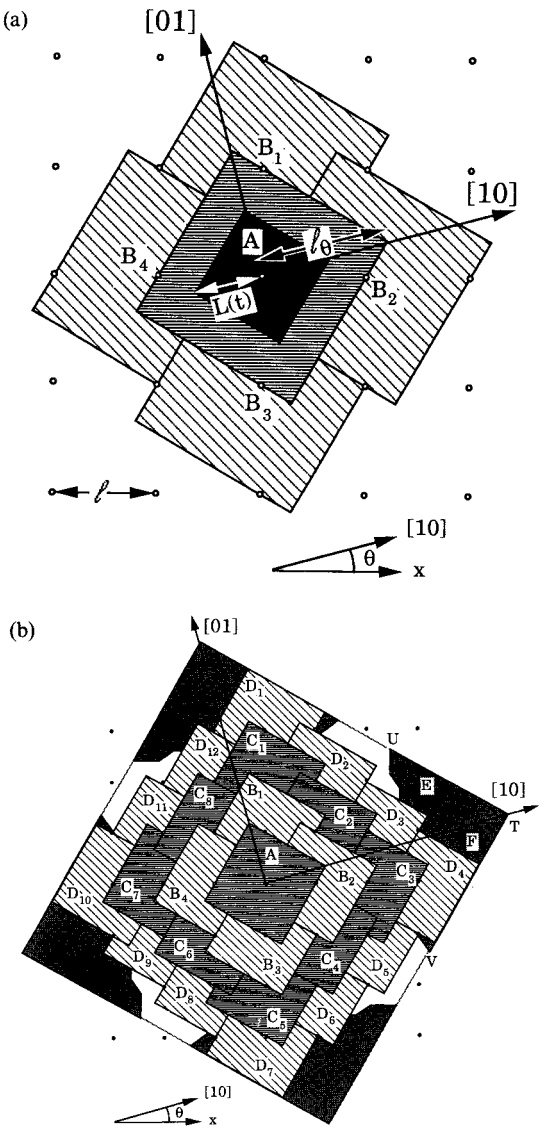

Fig. 7. (a) Details of the growth of one cellular automaton cell; (b) correction applied to the dendrite tip.

Firstly consider a CA site labeled "A" which has nucleated at a certain time, t_N [see Fig. 7(a)]. In two dimensions, its [10] orientation makes a certain angle, θ, with respect to the horizontal direction ($-45° < \theta < 45°$). Neglecting the incubation time during which the grain has a spherical or globulitic shape, the square which delimits the dendritic envelope [black square in Fig. 7(a)] has a half-diagonal, $L(t)$, which is simply given by the integral over time of the growth of the dendrite tip

$$L(t) = \int_{t_N}^{t} v[\Delta T(t')]\, dt'. \qquad (12)$$

This growth law, $v(\Delta T)$, which can be calculated by using the KGT model, is shown in Fig. 5 for two aluminium–silicon alloys of different compositions. At a certain time, t_B, the square grain will touch the four nearest neighbours, labeled "B1" to "B4". This

occurs for the fine-hatched square A whose half-diagonal, $L(t_B)$, is equal to the distance

$$\ell_\theta = \ell[\cos\theta + |\sin\theta|] \quad (13)$$

where ℓ is the spacing of the CA network.

Using a deterministic cellular automaton, the cell B's will solidify and their index will be set equal to that of the original nucleus A, when $L(t_B) = \ell_\theta$. However, the extension of a grain by branching mechanisms is not fully deterministic and thus the entrapment of the nearest neighbours might not occur precisely when $L(t) = \ell_\theta$ (i.e. when $t = t_B$). In order to reflect this probabilistic nature of grain extension, a given site B is imagined to be trapped by site A when a randomly generated number, r, is smaller than the probability, p_g, defined as

$$p_g = \frac{L(t)}{\ell_\theta}. \quad (14)$$

Let us now consider one of the B-sites which has been captured by the growth of A. Since entrapment usually occurs at a time, t'_B, which is smaller than t_B, due to the probabilistic procedure, then site B is assigned an initially negative half-diagonal at the time of capture in order to satisfy the growth kinetics law on average. This initial size is simply proportional to $[L(t'_B) - \ell_\theta]$. The index of the B site which has been captured is of course given by that of the parent cell A since the two cells correspond to the same grain and are thus characterized by the same crystallographic orientation. It should be noted that the deterministic growth of the grains (i.e. entrapment of neighbours when $L(t_B) = \ell_\theta$) and the probabilistic growth procedure (i.e. entrapment when $r < p_g$) did not produce significantly different results. The solid–liquid interface of the growing grain was noticed to be slightly more fuzzy when using the probabilistic cellular automaton, but the overall shape was the same.

On average, the initial size of the solidified nearest-neighbour site B's will be zero after a time increment $\delta t_B = t_B - t_N$, regardless of the growth procedure used (deterministic or probabilistic). When all of the B neighbours have their indices different to zero, the cell A is considered to be fully solid and its growth is no longer calculated. Proceeding further with the growth of the B-sites [see Fig. 7(b)], they will then capture the 8 C-sites after an average time increment, $\delta t_C = t_C - t_B$, and then these sites will trap the 12 D-sites after a time increment, $\delta t_D = t_D - t_C$, and so on. In this way, the original grain can propagate with an average velocity which is given by that of the dendrite tip. However, as shown in Fig. 7(b), this procedure clearly loses the original orientation of the nucleus: after three "generations", the solid site D's outline a square whose diagonals correspond to the directions of the CA network and not to the original $\langle 10 \rangle$ crystallographic directions of the grain. This is due to the fact that the growth kinetics of the grain is only conserved along the directions of the nearest neighbours. Such a result is shown in Fig. 8(a) for the square CA network shown in Figs 6(b) or 7 and the first nearest-neighbour configuration. This so-called von Neumann nearest-neighbour configuration [36] always produces squares whose diagonals are aligned with the directions of the square CA lattice. The situation may be improved by increasing the number of nearest-neighbour directions. Two examples are shown in Fig. 8(b) and (c) for the Moore configuration [36] (first- and second-nearest neighbours in a square lattice) and the hexagonal lattice used by Srolovitz *et al.* [25], respectively. For comparison, Fig. 8(g) shows a grain which would normally be produced when considering all of the cells which fall within an equivalent square centred on the original nucleus but whose diagonals are parallel to the $\langle 10 \rangle$ crystallographic orientations. Although the situation improves when considering 6 [hexagonal, Fig. 8(c)] or

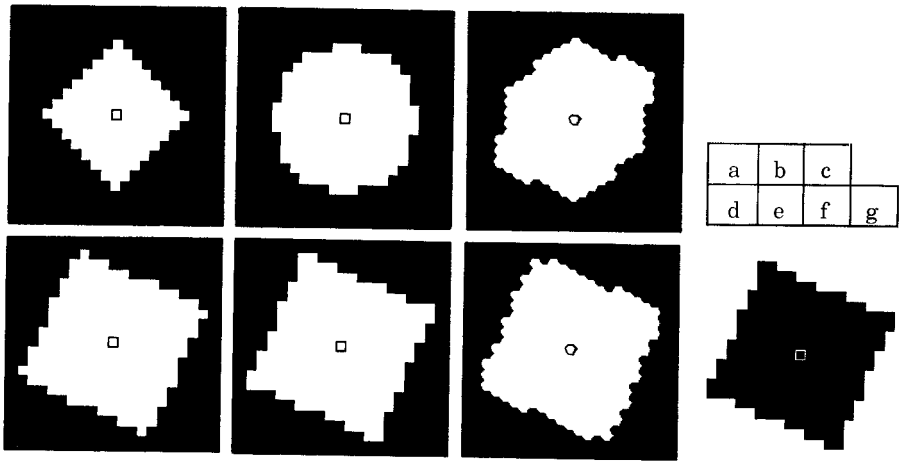

Fig. 8. A stage in the growth of a single dendritic grain, as calculated with the cellular automaton shown in Fig. 6(b), and three different neighbourhood configurations; (a) cubic von Neumann; (b) cubic Moore; and (c) hexagonal. The grains shown in (d–f) correspond to the result of cellular automaton calculation when a correction near to the dendrite tip is taken into account (see text). A calculation of the desired shape is shown in (g) for comparison.

8 [Moore cubic, Fig. 8(b)] neighbours, it is far from being satisfactory.

In order to avoid this network dependence of the CA model, a "dendrite tip correction" was added to the model. This correction is explained in Fig. 7(b). As mentioned before, all of the D-sites will be solid on average at a time, $t_D = t_N + (\delta t_B + \delta t_C + \delta t_D)$. However, after that time, the grain which would be obtained if the growth of the original nucleus was considered [see Fig. 8(g)] is a square whose diagonals are parallel to the $\langle 10 \rangle$ crystallographic orientations and whose half-length is given by

$$L(t_D) = \int_{t_N}^{t_D} v[\Delta T(t')]\, dt'. \qquad (15)$$

This square shape is also shown in Fig. 7(b). Without any correction, a whole region of the grain is missing near to the tip of the dendrites. In particular, the CA sites labeled E and F, which should have been captured by the original grain A, are still liquid. In order to avoid this situation, the position, T, of four dendrite tips of the original grain A is updated at each time step and a small triangular region, TUV, behind the tip is considered [see Fig. 7(b)]. The side of this rectangular triangle, TU or TV, is of the order of the spacing of the CA mesh, ℓ. Liquid cells which might have some probability of being captured by these moving triangles will have their index changed to that of the original nucleus and their radius initialized in a way simlar to that described before.

Figure 8(d–f) show the shape of the grain which is produced by using the CA model, including the tip correction, for the three network configurations: von Neumann, Moore and hexagonal. As can be seen, these shapes conserve the original crystallographic anisotropy, regardless of the network used. In the following section, the CA von Neumann model is applied to square sections of aluminium–silicon alloy billets.

4. RESULTS AND DISCUSSION

Figure 9 shows the evolution of the grain structure during solidification, and the final two-dimensional micrographs of an aluminium–7% silicon alloy, as computed using the CA model and various laws for nucleation in the bulk and at the surface of the casting. These two-dimensional ingots correspond to 5×5 mm^2 square-section billets† cast in a mould with the same cooling rate, $\dot{T}$. The number of CA points used for the simulation was 300×300, thus resulting in a resolution of about 15 μm. It is to be noted that this value is of the order of the secondary arm spacing and is thus well adapted to the modelling of the extension of grains by branching mechanisms. The dendrite growth kinetics of this alloy, which has been calculated using the KGT model, is the same in all three cases and is displayed in Fig. 5. The corresponding nucleation parameters and cooling rate for each specimen are listed in Table 1. The parameters listed for the nucleation site distributions are the following for both nucleation in the bulk volume (index "v") and at the surface of the mould (index "s"): ΔT_{max} is the centre of the Gaussian distribution, ΔT_σ is the standard deviation of the distribution and n is the total density of sites. Since the CA model is two-dimensional, standard stereological relationships were used to obtain values of n for the model from the values listed in Table 1. For the sake of simplicity, the parameters for nucleation at the mould wall were kept constant and only the centre of the distribution for nucleation in the bulk of the melt was varied in Fig. 9. The grains which appear in Fig. 9 have a colour which reflects their crystallographic orientation.

In Fig. 9(a), the columnar grains which originate from nuclei formed at the square surface of the mould can develop up to the centre of the ingot. This means that the average undercooling of the columnar dendrite tips is smaller than 10°C when they reach the centre of the ingot since the nucleation of equiaxed grains in the bulk liquid can only start at about 10°C (see Table 1). The numerous grains which are nucleated on the periphery of the ingot have random orientations, as can be seen from the different colours on the micrographs. As growth proceeds, only those grains with their $\langle 10 \rangle$ crystallographic orientation most closely aligned with the normal to the mould surface are selected. This selection mechanism is well reproduced by the CA model. It is not really based upon a minimum undercooling criterion, since the temperature of the specimen is uniform, but rather upon a "minimum travel" criterion: the dendrites extend faster into the volume of the ingot, from the mould wall, when their $\langle 10 \rangle$ orientation is perpendicular to the surface of the mould. The almost square cross-section of the remaining liquid, which can be seen during solidification in Fig. 9 (black zone), is due to the hypothesis of uniform temperature.

In the case of Fig. 9(b), the centre of the nucleation site distribution for equiaxed grains is closer to the liquidus of the alloy ($\Delta T_{v,max} = 8$°C, see Table 1) and equiaxed grains can form before the columnar region reaches the centre of the ingot. This trend is more pronounced when the centre of this distribution is only 6°C below the liquidus, as can be seen in Fig. 9(c). The columnar-to-equiaxed transition, which is nucleation-controlled in the case of a uniform temperature specimen, occurs at an earlier stage of solidification if the undercooling at which equiaxed grains nucleate in the bulk of the liquid is lower; as might be expected. The average size of the equiaxed grains in Fig. 9(b, c) is about the same since the distributions used to describe heterogeneous nucleation in the volume of the liquid are the same, and

†Due to a small distortion caused by the hard copy unit, the squares simulated on the computer screen appear as rectangles in Figs 9–11.

Table 1. Conditions used for the computations

	$\Delta T_{s,\max}$ [°C]	$\Delta T_{s,\sigma}$ [°C]	n_s [m^{-2}]	$\Delta T_{v,\max}$ [°C]	$\Delta T_{v,\sigma}$ [°C]	n_v [m^{-3}]	$\dot{T}$ [°C · s^{-1}]	c_0 [%]
Fig. 9(a)	0.5	0.1	2.5×10^8	10.5	0.1	5.5×10^{10}	−2.3	7
Fig. 9(b)	0.5	0.1	2.5×10^8	8.0	0.1	5.5×10^{10}	−2.3	7
Fig. 9(c)	0.5	0.1	2.5×10^8	6.0	0.1	5.5×10^{10}	−2.3	7
Fig. 10	0.5	0.1	2.5×10^8	8.0	0.1	5.5×10^{10}	−2.3	5
Fig. 11	0.5	0.1	2.5×10^8	8.0	0.1	5.5×10^{10}	−7.0	7

The site densities, n_s[m^{-2}] and n_v[m^{-3}], which are listed in this table apply to three-dimensional geometries. The following stereological relationships were used to deduce the corresponding values, n_s^*[m^{-1}] and n_v^*[m^{-2}], for the two-dimensional cellular automaton calculations

$$n_s = \frac{\pi}{4}[n_s^*]^2 \quad \text{and} \quad n_v = \sqrt{\frac{\pi}{6}}[n_v^*]^{3/2}.$$

very narrow; the only difference being the average position of these distributions, $\Delta T_{v,\max}$.

The microstructures which are produced by using this CA model very closely resemble those calculated by Brown and Spittle [22–24]. The advantage in this case is that the basic physical phenomena are incorporated into the model; in particular the growth kinetics of the dendrite tip and the distribution of crystallographic orientations. Therefore, the selection of columnar grains is based strictly upon a best-alignment criterion as observed *in situ* for organic alloys [26] or on metallographic cross-sections of metals [19, 20]. It can also be clearly seen in Fig. 9 that equiaxed grains grow with a square shape which, as explained before, is a simplification of the overall shape of real grains.

The value of this CA model is its ability to predict quantitatively the effect, of varying solidification conditions, upon the resultant microstructure. Two examples are provided by Figs 10 and 11. Figure 10 shows the final grain structure of an aluminium–5% silicon alloy solidified under the same conditions as the specimen shown in Fig. 9(b) (see Table 1), apart from the lower silicon concentration. As can be seen, the average distance, D_c, over which columnar dendrites can grow before they are stopped by equiaxed grains is larger than for the 7% silicon alloy. This can be explained quite easily by writing D_c explicitly for a grain which would grow with its [10] crystallographic orientation perpendicular to the surface of the mould

$$D_c = \int_{t_{N,c}}^{t_{N,e}} v[\Delta T(t')]\,dt' = \frac{1}{\dot{T}} \int_{T_{N,c}}^{T_{N,e}} v(T')\,dT'. \quad (16)$$

Here, $t_{N,c}$ and $t_{N,e}$ are *the* times† at which heterogeneous nucleation of grains occurs on the surface of the mould and in the bulk of the liquid, respectively. Since the corresponding temperatures, $T_{N,c}$ and $T_{N,e}$, as well as the cooling rate, $\dot{T}$, remain the same, then D_c is directly proportional to the growth kinetics law. For the less concentrated alloy, the growth kinetics of the dendrite tips is faster, as can be seen in Fig. 5. Thus, for the same cooling rate, the dendrites grow faster at a given undercooling and the extent, D_c, of the columnar grains, as calculated with equation (16) is larger. This behaviour, which is clearly seen by the comparison of Figs 9(b) and 10, is in qualitative agreement with experimental observations [37] and with the results of Brown and Spittle [22–24]. However, in real experiments, the solidification conditions are such that, when dendrites are growing faster, the associated latent heat release will partially modify the cooling rate and will thus reduce somewhat the effect of the alloy concentration upon the CET. It should be emphasized here that the observed difference between Figs 9(b) and 10 is due only to the growth kinetics and not to variations in the cooling rate or in the nucleation parameters.

The microstructure shown in Fig. 11 corresponds to the same aluminium–7% silicon alloy of Fig. 9(b), but after solidification at a cooling rate which was three times higher (see Table 1). As can be seen, the size of the equiaxed grains is roughly the same as those of Figs 9 and 10 because the width of the nucleation site distribution is very narrow. Therefore, all the potential nucleation sites become active and give the same final grain size. The use of a larger distribution will clearly change this situation, as already predicted by deterministic models of solidification [6]. It is interesting to note that the extent of the columnar region is drastically reduced upon increasing the cooling rate [compare Figs 9(b) and 11]. It should be kept in mind that a uniform temperature has been assumed to exist in both cases, an hypothesis which becomes less valid as the cooling rate, or the Biot number, is increased. Nevertheless, this behaviour can again be explained quite easily with the help of equation (16) since the extension of the columnar grains, D_c, is inversely proportional to the cooling rate, $\dot{T}$.

†Heterogeneous nucleation occurs at a unique time when the corresponding nucleation site distribution reduces to a Dirac function.

Fig. 9 (*facing page*). Development of the grain structure during the solidification of an Al–7% Si specimen, as calculated using the two-dimensional cellular automaton. The growth kinetics of this alloy is shown in Fig. 5 and the cooling rate is −2.3 K/s. The different cases (a–c) correspond to the nucleation parameters listed in Table 1.

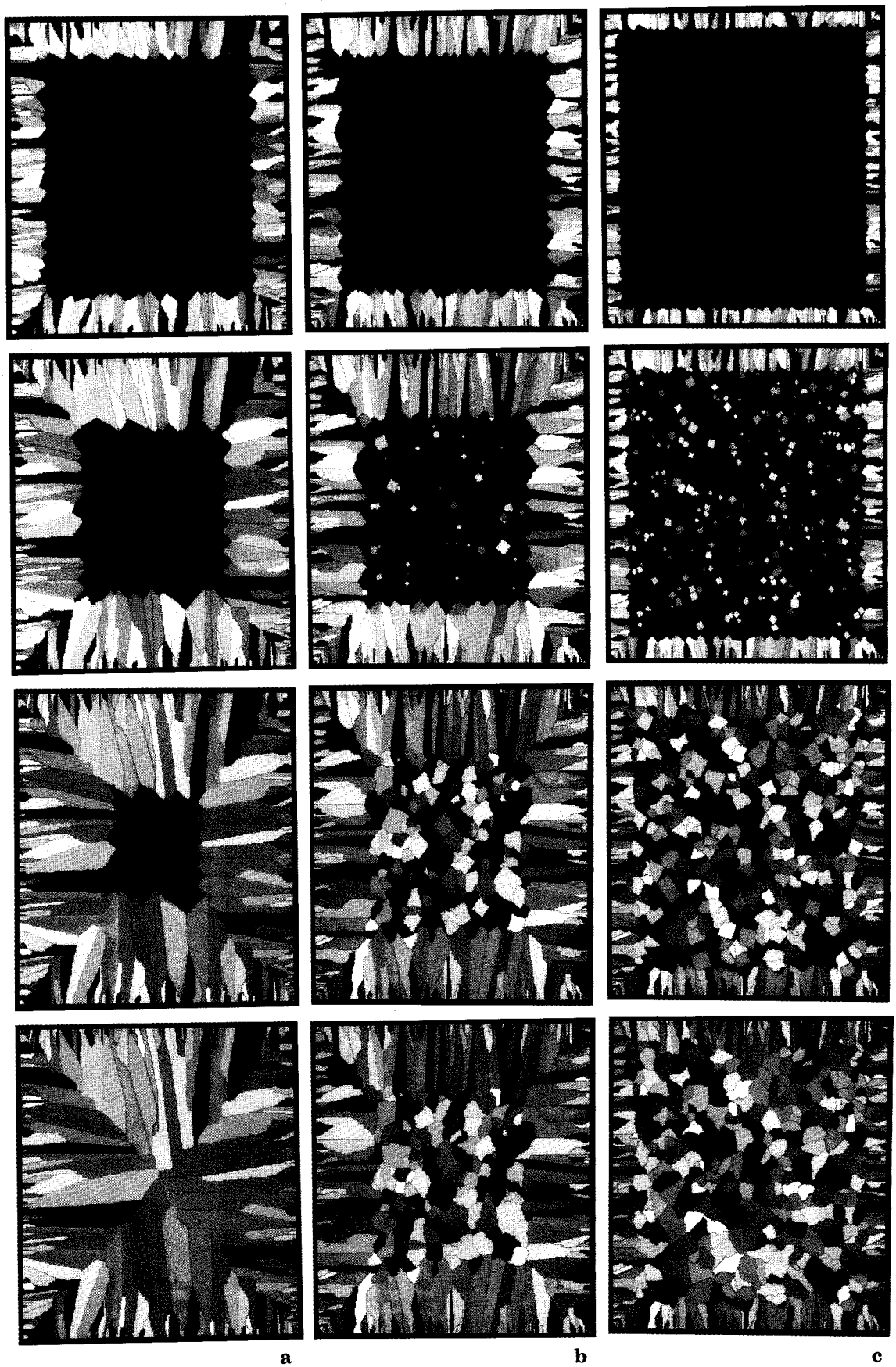

Fig. 9

Fig. 10. Final grain structure of an Al–5% Si specimen of uniform temperature, as calculated using the two-dimensional cellular automaton. The parameters for this calculation are the same as those of Fig. 9(b), except for the initial concentration of the alloy.

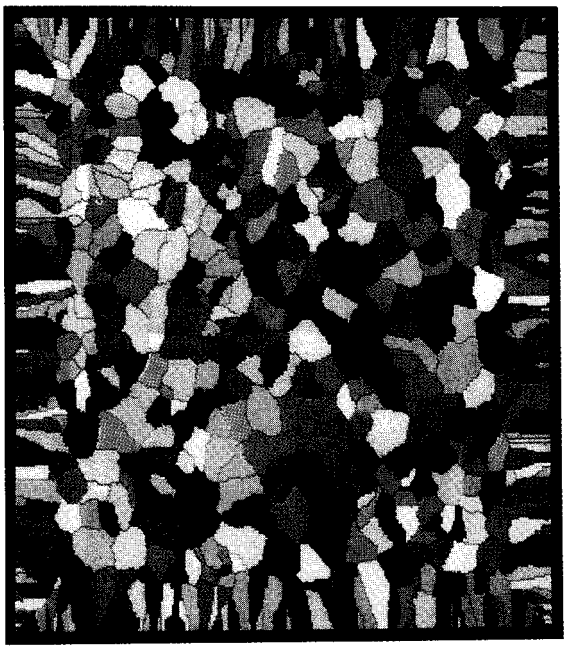

Fig. 11. Final grain structure of an Al–7% Si specimen of uniform temperature as calculated using the two-dimensional cellular automaton. The cooling rate in this case is tripled with respect to that of Fig. 9(b) ($\dot{T} = -7.0$ K/s).

A final comment should be made regarding the computation time. Each of the microstructures shown in Figs 9–11 was computed using 90,000 cells on the Apollo DN10000 workstation. The total computation time was 30 min.

6. CONCLUSIONS

A cellular automaton has been developed for simulating the solidification of dendritic alloys. This model, which at the moment applies only to specimens with a uniform temperature, is based upon the physical mechanisms of solidification. In particular, heterogeneous nucleation at the mould surface and in the bulk of the liquid are taken into account via the use of nucleation site distributions. These distributions, which are the same as those previously developed for deterministic approaches to solidification, can only be deduced from experimental observations. The model also accounts for the growth kinetics of the dendrite tips, for the branching mechanisms which lead to the formation, selection and extension of grains, and for the preferential growth directions. Though the microstructures are quite similar to those produced by Brown and Spittle [22–24], the selection of columnar grains in the present model is based upon a minimum undercooling criterion (or best alignment criterion in the case of a uniform temperature) and reflects the anisotropy of the growth of dendritic alloys. Furthermore, the CET can be predicted quantitatively since the growth kinetics of the dendrite tip is directly included in the model.

The advantage of the CA model presented here is that the final computed microstructures can be directly compared with real micrographic cross-sections. However, it should be kept in mind that the model is two-dimensional at the moment and isothermal. If this last hypothesis was to be removed, the remaining liquid seen in Fig. 9 during growth (black region in the centre of the ingot) would no longer have a square shape but would be delimited by the liquidus isotherm. Accordingly, the shape of the grains would be slightly different. Similarly, when considering non-uniform temperature conditions, the grains themselves will depart from a square shape since each CA site will be characterized by a different temperature history.

Another feature which could be very helpful when comparing computed and experimental microstructures would be the crystallographic texture. As predicted by the CA model, the orientation distribution of the columnar grains narrows as the distance from the mould surface increases, due to the selection of those grains which are best aligned with the heat flow direction. A quantitative comparison between textures calculated using the cellular automaton and those observed in directionally solidified specimens [19] could be made in order to check the accuracy of the model.

Finally, several important solidification problems could be answered with the aid of the CA model provided that it was adapted to non-uniform temperature situations. Among other features that might be treated are the selection mechanism which operates in a grain selector for single-crystal turbine blade applications, the extension of grains in open regions of liquid, the CET transition in continuous casting, grain formation in welding and laser remelting, etc. An advantage of CA models is that, unlike FEM or FDM calculations, the CPU time is almost linear in the number of cells. Therefore, especially with the appearance of very powerful workstations on the market, it is believed that this type of calculation will give realistic computation times while providing metallurgists and foundry engineers with a very useful tool for the prediction of grain structures in solidification processes.

Acknowledgements—The authors would like to thank the SNECMA company for their financial aid, Professor W. Kurz and Ch. Charbon for reviewing and improving this manuscript.

REFERENCES

1. M. Rappaz, M. Ozgu and K. Mahin (editors), *Modeling of Casting, Welding and Advanced Solidification Processes*. TMS, Warrendale, Pa (1991).
2. W. D. Bennon and F. P. Incropera, *Int. J. Heat Mass Transfer* **30,** 2161, 2171 (1987).
3. V. R. Voller, A. D. Brent and C. Prakash, *Int. J. Heat Mass Transfer* **32,** 1719 (1989).
4. S. Ganesan and D. R. Poirier, *Metall. Trans.* **21B,** 173 (1990).
5. J. Ni and C. Beckermann, *Metall. Trans.* **22B,** 349 (1991).
6. M. Rappaz, *Int. Mater. Rev.* **34,** 93 (1989).
7. W. Kurz, B. Giovanola and R. Trivedi, *Acta metall.* **34,** 823 (1986).
8. R. Trivedi, P. Magnin and W. Kurz, *Acta metall.* **35,** 971 (1987).
9. W. A. Johnson and R. F. Mehl, *Trans. Am. Inst. Min. Engrs* **135,** 416 (1939).
10. M. Avrami, *J. chem. Phys.* **8,** 212 (1940).
11. C. W. Price, *Acta metall.* **35,** 1377 (1987).
12. Zou Jie, Ph.D. thesis, Ecole Polytechnique Fédérale de Lausanne, Switzerland (1988).
13. F. Mampaey, in *Euromat '91* (edited by T. W. Clyne and P. J. Withers), 531A, p. 182. The Inst. of Materials, London (1992).
14. K. C. Su, I. Ohnaka, I. Yamauchi and T. Fukusako, *MRS Symp. Proc.* **34,** 181 (1985).
15. D. M. Stefanescu and C. S. Kanetkar, *AFS Trans.* **95,** (1987).
16. Ph. Thévoz, J. L. Desbiolles and M. Rappaz, *Metall. Trans.* **20A,** 311 (1989).
17. R. Kuklinski, R. N. Smith, M. E. Glicksman and S. Marsh, in Ref. [1], p. 411.
18. W. Kurz and D. J. Fisher, *Fundamentals of Solidification*. Trans. Tech. Aedermannsdorf, Switzerland (1989).
19. B. Chalmers, *Principles of Solidification*. Wiley, New York (1964).
20. M. Rappaz and E. Blank, *J. Cryst. Growth* **74,** 67 (1986).
21. S. C. Flood and J. D. Hunt, *J. Cryst. Growth* **82,** 543, 552 (1987).
22. S. G. R. Brown and J. A. Spittle, in Ref. [1], p. 395.

23. J. A. Spittle and S. G. R. Brown, *Acta metall.* **37,** 1803 (1989).
24. S. G. R. Brown and J. A. Spittle, *Mater. Sci. Tech.* **5,** 362 (1989).
25. M. P. Anderson, D. J. Srolovitz, G. S. Grest and P. S. Sahni, *Acta metall.* **32,** 783 (1984). See also by these authors: *Acta metall.* **32,** 793 (1984); **32,** 1429 (1984); **33,** 509 (1985); **33,** 2233 (1985).
26. H. Esaka, W. Kurz and R. Trivedi, in *Solidification Processing* (edited by J. Beech and H. Jones). Inst. Metals, London, p. 198 (1988).
27. M. McLean, *Directionally Solidificed Materials for High Temperature Service.* The Metals Society, London (1983).
28. D. G. McCartney, *Int. Mater. Rev.* **34,** 247 (1989).
29. K. A. Jackson, J. D. Hunt, D. R. Uhlman and T. P. Seward III, *Trans. metall. Soc. AIME* **236,** 149 (1966).
30. I. Maxwell and A. Hellawell, *Acta metall.* **23,** 229 (1975).
31. D. Turnbul, *J. chem. Phys.* **18,** 198 (1949).
32. W. Oldfield, *Trans. Am. Soc. Metals* **59,** 945 (1966).
33. J. Lacaze, M. Castro and G. Lesoult, in *Euromat '89* (edited by H. E. Exner and V. Schumaker), p. 147. DGM, Oberursel (1990).
34. J. Lipton, M. E. Glicksman and W. Kurz, *Mater. Sci. Engng* **65,** 57 (1984).
35. E. Ferain, Diploma work, Ecole Polytechnique Fédérale de Lausanne (1986).
36. H. W. Hesselbarth and I. R. Göbel, *Acta metall. mater.* **39,** 2135 (1991).
37. C. A. Tarshis, J. L. Walker and J. W. Rutter, *Metall. Trans.* **2,** 2589 (1971).